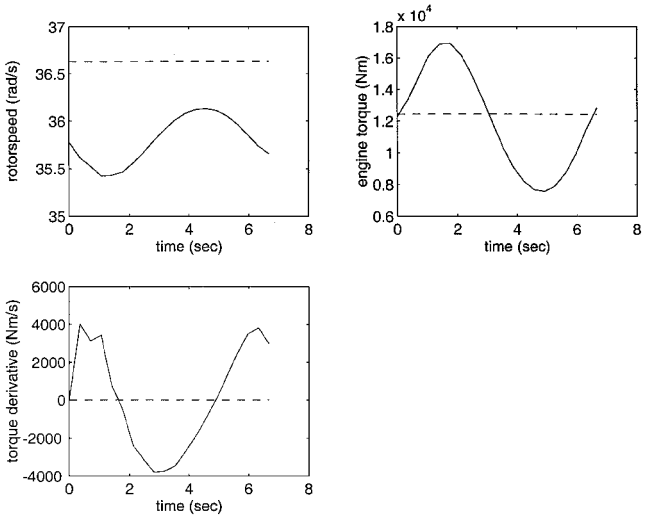

Fig. 2 Comparison between inverse simulation results generated by Genisa/Hibrom I and II (hurdle hop: V_f = 40 kn, h = 5 m, s = 150 m); time step: two turns of main rotor. ——, Genisa/Hibrom II, and – – –, Genisa/Hibrom I.

behavior is that a minimum interval corresponding to two turns of the main rotor is required to allow the transient engine dynamics to settle down toward a new steady state following each application of the controls. The time constant associated with a first-order approximation to the engine governor model is typically 0.397 s. This is more than double the time interval of 0.1755 s that corresponds to one full turn of the main rotor. This explanation can be verified by reducing the engine model time constants τ_{e1}, τ_{e2}, and τ_{e3} to 1% of their nominal values. The results improve, and a control application interval of once per revolution produces smooth control time histories and engine states.

V. Conclusions

An engine governor model has been successfully incorporated into the individual blade rotor model Hibrom for helicopter inverse simulation. Hence, the rotorspeed is now a degree of freedom within the modeled system.

A series of modifications have been made to the solution algorithm Genisa to accommodate the variation in rotorspeed. In particular, the control application interval is now recalculated iteratively at each time step. This is necessary to match the rotor periodicity that is inherent in the individual blade rotor model. In addition, the control application interval must be sufficiently long to allow the transient dynamics to settle; otherwise algorithm failure can occur.

The addition of the rotorspeed degree of freedom does not significantly affect the predicted control time histories for the maneuver considered in this study. However, as the boundaries of the flight envelope are approached, it may be expected that the enhanced rotor model will be closer to predicting actual flight behavior. Furthermore, with the introduction of the rotorspeed degree of freedom, it will now be possible to improve simulation fidelity by including other blade degrees of freedom.

References

[1]Rutherford, S., and Thomson, D. G., "Helicopter Inverse Simulation Incorporating an Individual Blade Rotor Model," *Journal of Aircraft*, Vol. 34, No. 5, 1997, pp. 627–634.

[2]Hess, R. A., Gao, C., and Wang, S. H., "Generalized Technique for Inverse Simulation Applied to Aircraft Maneuvers," *Journal of Guidance, Control, and Dynamics*, Vol. 14, No. 5, 1991, pp. 920–926.

[3]Padfield, G. D., "A Theoretical Model of Helicopter Flight Mechanics for Application to Piloted Simulation," Royal Aircraft Establishment, TR 81048, Bedford, England, U.K., April 1981.

[4]Rutherford, S., "Simulation Techniques for the Study of the Manoeuvring of Advanced Rotorcraft Configurations," Ph.D. Dissertation, Dept. of Aerospace Engineering, Univ. of Glasgow, Glasgow, Scotland, U.K., March 1997.

Structural Dynamics and Quasistatic Aeroelastic Equations of Motion

John R. Dykman* and William P. Rodden†
The Boeing Company, Long Beach, California 90807-5309

Introduction

THE quasistatic aeroelastic equations of motion of a flight vehicle include all of the static effects of flexibility and assume that there are no structural dynamic effects, i.e., the vehicle is regarded a point vehicle with six degrees of freedom. Thus, all points of the structure are in phase with the motions of a reference point, e.g., the center of gravity or the quarter point of the mean aerodynamic reference chord. The dynamic effects of structural modes cannot be included simply by adding the modal equations of motion to couple with the quasistatic equations, as has been incorrectly suggested by Rodden and Love.[1] The correct formulation begins with the mean axis equations of motion to which the modal dynamic equations are added with all appropriate aeroelastic coupling.[2] Many modes must be included to account accurately for static aeroelastic behavior, but because not all of these are necessary to account for the dynamic response, the high-frequency modes can be eliminated by residualization.[3]

Residualization of the Aeroelastic Equations of Motion

The fundamental equation of motion of a linear aeroelastic system in generalized (modal) coordinates is given in Eq. (1). The system free vibration mode shapes are the generalized coordinates $\boldsymbol{q}$ and the control surface inputs are generalized coordinates $\boldsymbol{q}^c$.

$$\boldsymbol{M}\ddot{\boldsymbol{q}} + \boldsymbol{C}\dot{\boldsymbol{q}} + \boldsymbol{K}\boldsymbol{q} = \bar{q}\boldsymbol{Q}_0(M) + \mathcal{F}^{-1}[\bar{q}\boldsymbol{Q}(M,k)\boldsymbol{q}] - \boldsymbol{M}^c\ddot{\boldsymbol{q}}^c + \mathcal{F}^{-1}[\bar{q}\boldsymbol{Q}^c(M,k)\boldsymbol{q}^c] + \boldsymbol{W} \tag{1}$$

The generalized structural mass, damping, and stiffness matrices are $\boldsymbol{M}$, $\boldsymbol{C}$, and $\boldsymbol{K}$, respectively; $\boldsymbol{W}$ is a vector of weight and static unbalance components adjusted for the trim pitch angle of the mean axes. The coupled control surface generalized structural mass matrix is $\boldsymbol{M}^c$, and the control surface stiffness and damping are neglected. The generalized aerodynamic coefficients $\boldsymbol{Q}_0(M)$ are intercept values for incidence, twist, and camber and are functions of the Mach number M. The generalized unsteady aerodynamic coefficients $\boldsymbol{Q}(M,k)$ and the coupled control surface generalized unsteady aerodynamic coefficients $\boldsymbol{Q}^c(M,k)$ in the frequency domain are functions of Mach number and reduced frequency k, where $k = \omega\bar{c}/2V$ in which ω is the angular frequency, $\bar{c}$ is the reference chord, and V is the flight velocity. The aerodynamic force is scaled by dynamic pressure $\bar{q}$, where $\bar{q} = \rho V^2/2$ in which ρ is the atmospheric density. $\mathcal{F}^{-1}[\,]$ represents the inverse Fourier transform of the quantity in brackets. The generalized unsteady aerodynamic coefficients are complex and can be separated into their real and imaginary parts to obtain an approximation in the time domain as

$$\mathcal{F}^{-1}[\bar{q}\boldsymbol{Q}(M,k)\boldsymbol{q}] = \mathcal{F}^{-1}\{\bar{q}[{}^R\boldsymbol{Q}(M,k)]\boldsymbol{q} + \bar{q}(\bar{c}/2V)[{}^I\boldsymbol{Q}(M,k)/k]i\omega\boldsymbol{q}\} \approx \bar{q}\boldsymbol{A}\boldsymbol{q} + \bar{q}(\bar{c}/2V)\boldsymbol{B}\dot{\boldsymbol{q}} \tag{2}$$

The coefficients are obtained from an unsteady aerodynamic theory such as the doublet-lattice method,[4,5] where $\boldsymbol{A}$ is the real part of the generalized aerodynamic force (GAF) matrix and $\boldsymbol{B}$ is the imaginary

Received 7 July 1998; revision received 26 November 1999; accepted for publication 23 January 2000.

*Principal Engineer of Stability, Control, and Flying Qualities. Member AIAA.

†Consultant.

part of the GAF matrix divided by k for a selected Mach number and reduced frequency. Likewise, for the control surfaces

$$\mathcal{F}^{-1}[\bar{q}\boldsymbol{Q}^c(M,k)\boldsymbol{q}^c] = \mathcal{F}^{-1}\{\bar{q}[{}^R\boldsymbol{Q}^c(M,k)]\boldsymbol{q}^c + \bar{q}(\bar{c}/2V)[{}^I\boldsymbol{Q}^c(M,k)/k]i\omega\boldsymbol{q}^c\} \approx \bar{q}\boldsymbol{A}^c\boldsymbol{q}^c + \bar{q}(\bar{c}/2V)\boldsymbol{B}^c\dot{\boldsymbol{q}}^c \tag{3}$$

This approximation makes the GAFs invariant with frequency. For a quasistatic aerodynamic assumption these coefficients are evaluated at a low value of k such as 0.001. With these assumptions Eqs. (1–3) can be combined to give Eq. (4), where the aerodynamic coefficients are shown as constants.

$$\boldsymbol{M}\ddot{\boldsymbol{q}} + \boldsymbol{C}\dot{\boldsymbol{q}} + \boldsymbol{K}\boldsymbol{q} = \bar{q}\boldsymbol{Q}_0 + \bar{q}\boldsymbol{A}\boldsymbol{q} + \bar{q}(\bar{c}/2V)\boldsymbol{B}\dot{\boldsymbol{q}} - \boldsymbol{M}^c\ddot{\boldsymbol{q}}^c + \bar{q}\boldsymbol{A}^c\boldsymbol{q}^c + \bar{q}(\bar{c}/2V)\boldsymbol{B}^c\dot{\boldsymbol{q}}^c + \boldsymbol{W} \tag{4}$$

If the generalized coordinates are partitioned into those for rigid body modes (R), the flexible dynamic modes (D), and the flexible static modes (S), then Eq. (4) can be rewritten as Eq. (5).

$$\begin{bmatrix} \boldsymbol{M}_R & 0 & 0 \\ 0 & \boldsymbol{M}_D & 0 \\ 0 & 0 & \boldsymbol{M}_S \end{bmatrix} \begin{Bmatrix} \ddot{\boldsymbol{q}}_R \\ \ddot{\boldsymbol{q}}_D \\ \ddot{\boldsymbol{q}}_S \end{Bmatrix} + \begin{bmatrix} 0 & 0 & 0 \\ 0 & \boldsymbol{C}_D & 0 \\ 0 & 0 & \boldsymbol{C}_S \end{bmatrix} \begin{Bmatrix} \dot{\boldsymbol{q}}_R \\ \dot{\boldsymbol{q}}_D \\ \dot{\boldsymbol{q}}_S \end{Bmatrix} + \begin{bmatrix} 0 & 0 & 0 \\ 0 & \boldsymbol{K}_D & 0 \\ 0 & 0 & \boldsymbol{K}_S \end{bmatrix} \begin{Bmatrix} \boldsymbol{q}_R \\ \boldsymbol{q}_D \\ \boldsymbol{q}_S \end{Bmatrix} = \bar{q} \begin{Bmatrix} \boldsymbol{Q}_0 \\ 0 \\ 0 \end{Bmatrix}$$

$$+ \bar{q} \begin{bmatrix} \boldsymbol{A}_R & \boldsymbol{A}_{\mathrm{RD}} & \boldsymbol{A}_{\mathrm{RS}} \\ \boldsymbol{A}_{\mathrm{DR}} & \boldsymbol{A}_D & \boldsymbol{A}_{\mathrm{DS}} \\ \boldsymbol{A}_{\mathrm{SR}} & \boldsymbol{A}_{\mathrm{SD}} & \boldsymbol{A}_S \end{bmatrix} \begin{Bmatrix} \boldsymbol{q}_R \\ \boldsymbol{q}_D \\ \boldsymbol{q}_S \end{Bmatrix} + \bar{q}\left(\frac{\bar{c}}{2V}\right) \begin{bmatrix} \boldsymbol{B}_R & \boldsymbol{B}_{\mathrm{RD}} & \boldsymbol{B}_{\mathrm{RS}} \\ \boldsymbol{B}_{\mathrm{DR}} & \boldsymbol{B}_D & \boldsymbol{B}_{\mathrm{DS}} \\ \boldsymbol{B}_{\mathrm{SR}} & \boldsymbol{B}_{\mathrm{SD}} & \boldsymbol{B}_S \end{bmatrix} \begin{Bmatrix} \dot{\boldsymbol{q}}_R \\ \dot{\boldsymbol{q}}_D \\ \dot{\boldsymbol{q}}_S \end{Bmatrix} - \begin{bmatrix} \boldsymbol{M}_R^c \\ \boldsymbol{M}_D^c \\ \boldsymbol{M}_S^c \end{bmatrix} \{\ddot{\boldsymbol{q}}^c\}$$

$$+ \bar{q} \begin{bmatrix} \boldsymbol{A}_R^c \\ \boldsymbol{A}_D^c \\ \boldsymbol{A}_S^c \end{bmatrix} \{\boldsymbol{q}^c\} + \bar{q}\left(\frac{\bar{c}}{2V}\right) \begin{bmatrix} \boldsymbol{B}_R^c \\ \boldsymbol{B}_D^c \\ \boldsymbol{B}_S^c \end{bmatrix} \{\dot{\boldsymbol{q}}^c\} + \begin{Bmatrix} \boldsymbol{W} \\ 0 \\ 0 \end{Bmatrix} \tag{5}$$

This equation describes the entire aeroelastic system and can include a large number of the free vibration modes of the system. The flexible modes are partitioned into groups called "dynamic" and "static" for convenience in the following development. The "dynamic" modes are those modes whose dynamic effect is kept in subsequent analyses. The "static" modes are those higher frequency modes whose dynamic effect is neglected but whose static effect is kept in the subsequent analyses. The dimensional characteristics of the rigid body partitions $\boldsymbol{A}_R$ and $\boldsymbol{B}_R$ can be illustrated in the longitudinal case with plunging and pitching degrees of freedom (DOF)

$$\boldsymbol{q}_R = \begin{Bmatrix} z \\ \theta \end{Bmatrix}, \qquad \boldsymbol{A}_R = S \begin{bmatrix} 0 & C_{z_\alpha} \\ 0 & C_{m_\alpha}\bar{c} \end{bmatrix}$$

$$\boldsymbol{B}_R = S \begin{bmatrix} 2C_{z_\alpha} & \bar{c} & C_{z_{\dot{\alpha}}} + C_{z_q} \\ 2C_{m_\alpha} & & \left(C_{m_{\dot{\alpha}}} + C_{m_q}\right)\bar{c} \end{bmatrix}$$

where S is the reference area and customary notation is used for the stability derivatives.

To reduce the size of the problem, the static modes are residualized by retaining their deflections but eliminating their velocities and accelerations.[3] This is accomplished by setting $\dot{\boldsymbol{q}}_S = \ddot{\boldsymbol{q}}_S = 0$ in Eq. (5) and solving for the flexible static modal deflections $\boldsymbol{q}_S$, which are

$$\boldsymbol{q}_S = \bar{q}(\boldsymbol{K}_S - \bar{q}\boldsymbol{A}_S)^{-1}[\boldsymbol{A}_{\mathrm{SR}} \vdots \boldsymbol{A}_{\mathrm{SD}}] \begin{Bmatrix} \boldsymbol{q}_R \\ \cdots \\ \boldsymbol{q}_D \end{Bmatrix} + \bar{q}(\bar{c}/2V)(\boldsymbol{K}_S - \bar{q}\boldsymbol{A}_S)^{-1}[\boldsymbol{B}_{\mathrm{SR}} \vdots \boldsymbol{B}_{\mathrm{SD}}] \begin{Bmatrix} \dot{\boldsymbol{q}}_R \\ \cdots \\ \dot{\boldsymbol{q}}_D \end{Bmatrix} - (\boldsymbol{K}_S - \bar{q}\boldsymbol{A}_S)^{-1}\boldsymbol{M}_S^c\ddot{\boldsymbol{q}}^c + \bar{q}(\boldsymbol{K}_S - \bar{q}\boldsymbol{A}_S)^{-1}\boldsymbol{A}_S^c\boldsymbol{q}^c + \bar{q}(\bar{c}/2V)(\boldsymbol{K}_S - \bar{q}\boldsymbol{A}_S)^{-1}\boldsymbol{B}_S^c\dot{\boldsymbol{q}}^c \tag{6}$$

Eliminating $\boldsymbol{q}_S$ from Eq. (5) gives

$$\begin{bmatrix} \boldsymbol{M}_R & 0 \\ 0 & \boldsymbol{M}_D \end{bmatrix} \begin{Bmatrix} \ddot{\boldsymbol{q}}_R \\ \ddot{\boldsymbol{q}}_D \end{Bmatrix} + \begin{bmatrix} 0 & 0 \\ 0 & \boldsymbol{C}_D \end{bmatrix} \begin{Bmatrix} \dot{\boldsymbol{q}}_R \\ \dot{\boldsymbol{q}}_D \end{Bmatrix} + \begin{bmatrix} 0 & 0 \\ 0 & \boldsymbol{K}_D \end{bmatrix} \begin{Bmatrix} \boldsymbol{q}_R \\ \boldsymbol{q}_D \end{Bmatrix} = \bar{q} \begin{Bmatrix} \boldsymbol{Q}_0 \\ 0 \end{Bmatrix} + \bar{q} \begin{bmatrix} \bar{\boldsymbol{A}}_R & \bar{\boldsymbol{A}}_{\mathrm{RD}} \\ \bar{\boldsymbol{A}}_{\mathrm{DR}} & \bar{\boldsymbol{A}}_D \end{bmatrix} \begin{Bmatrix} \boldsymbol{q}_R \\ \boldsymbol{q}_D \end{Bmatrix}$$

$$+ \bar{q}\left(\frac{\bar{c}}{2V}\right) \begin{bmatrix} \bar{\boldsymbol{B}}_R & \bar{\boldsymbol{B}}_{\mathrm{RD}} \\ \bar{\boldsymbol{B}}_{\mathrm{DR}} & \bar{\boldsymbol{B}}_D \end{bmatrix} \begin{Bmatrix} \dot{\boldsymbol{q}}_R \\ \dot{\boldsymbol{q}}_D \end{Bmatrix} - \begin{bmatrix} \bar{\boldsymbol{M}}_R^c \\ \bar{\boldsymbol{M}}_D^c \end{bmatrix} \{\ddot{\boldsymbol{q}}^c\} + \bar{q} \begin{bmatrix} \bar{\boldsymbol{A}}_R^c \\ \bar{\boldsymbol{A}}_D^c \end{bmatrix} \{\boldsymbol{q}^c\} + \bar{q}\left(\frac{\bar{c}}{2V}\right) \begin{bmatrix} \bar{\boldsymbol{B}}_R^c \\ \bar{\boldsymbol{B}}_D^c \end{bmatrix} \{\dot{\boldsymbol{q}}^c\} + \begin{Bmatrix} \boldsymbol{W} \\ 0 \end{Bmatrix} \tag{7}$$

Generic forms for the various barred partitions in the preceding equation can be written as follows. For the singly subscripted partitions of $\boldsymbol{A}$ or $\boldsymbol{B}$,

$$\bar{\boldsymbol{P}}_l = \boldsymbol{P}_l + \bar{q}\boldsymbol{A}_{lS}(\boldsymbol{K}_S - \bar{q}\boldsymbol{A}_S)^{-1}\boldsymbol{P}_{Sl} \tag{8}$$

and for the doubly subscripted partitions

$$\bar{\boldsymbol{P}}_{mn} = \boldsymbol{P}_{mn} + \bar{q}\boldsymbol{A}_{mS}(\boldsymbol{K}_S - \bar{q}\boldsymbol{A}_S)^{-1}\boldsymbol{P}_{Sn} \tag{9}$$

where $\boldsymbol{P}$ denotes $\boldsymbol{A}$ or $\boldsymbol{B}$, l and m denote R or D, and n denotes D or R. For the control system partitions the generic form is singly subscripted as

$$\bar{\boldsymbol{P}}_l^c = \boldsymbol{P}_l^c + \bar{q}\boldsymbol{A}_{lS}(\boldsymbol{K}_S - \bar{q}\boldsymbol{A}_S)^{-1}\boldsymbol{P}_S^c \tag{10}$$

where $\boldsymbol{P}^c$ denotes $\boldsymbol{M}^c$, $\boldsymbol{A}^c$, or $\boldsymbol{B}^c$ and l denotes R or D.

The quasistatic aeroelastic (QSAE) solution is obtained by keeping just the deflections of the dynamic modes and eliminating their velocities and accelerations. This is accomplished by setting $\dot{\boldsymbol{q}}_D = \ddot{\boldsymbol{q}}_D = 0$ in Eq. (7) and is equivalent to residualizing all of the flexible modes, both static and dynamic. In this case

$$\boldsymbol{q}_D = \bar{q}(\boldsymbol{K}_D - \bar{q}\bar{\boldsymbol{A}}_D)^{-1}\bar{\boldsymbol{A}}_{\mathrm{DR}}\boldsymbol{q}_R + \bar{q}(\bar{c}/2V)(\boldsymbol{K}_D - \bar{q}\bar{\boldsymbol{A}}_D)^{-1}\bar{\boldsymbol{B}}_{\mathrm{DR}}\dot{\boldsymbol{q}}_R - (\boldsymbol{K}_D - \bar{q}\bar{\boldsymbol{A}}_D)^{-1}\bar{\boldsymbol{M}}_D^c\ddot{\boldsymbol{q}}^c + \bar{q}(\boldsymbol{K}_D - \bar{q}\bar{\boldsymbol{A}}_D)^{-1}\bar{\boldsymbol{A}}_D^c\boldsymbol{q}^c + \bar{q}(\bar{c}/2V)(\boldsymbol{K}_D - \bar{q}\bar{\boldsymbol{A}}_D)^{-1}\bar{\boldsymbol{B}}_D^c\dot{\boldsymbol{q}}^c \tag{11}$$

and Eq. (7) reduces to

$$\boldsymbol{M}_R\ddot{\boldsymbol{q}}_R = \bar{q}\boldsymbol{Q}_0 + \bar{q}\bar{\bar{\boldsymbol{A}}}_R\boldsymbol{q}_R + \bar{q}(\bar{c}/2V)\bar{\bar{\boldsymbol{B}}}_R\dot{\boldsymbol{q}}_R - \bar{\bar{\boldsymbol{M}}}_R^c\ddot{\boldsymbol{q}}^c + \bar{q}\bar{\bar{\boldsymbol{A}}}_R^c\boldsymbol{q}^c + \bar{q}(\bar{c}/2V)\bar{\bar{\boldsymbol{B}}}_R^c\dot{\boldsymbol{q}}^c + \boldsymbol{W} \tag{12}$$

with the generic expressions for the doubly barred partitions written as

$$\bar{\bar{P}}_R = \bar{P}_R + \bar{q}\bar{A}_{\mathrm{RD}}(K_D - \bar{q}\bar{A}_D)^{-1}\bar{P}_{\mathrm{DR}} \tag{13}$$

where $\bar{P}_R$ denotes $\bar{A}_R$ or $\bar{B}_R$ and $\bar{P}_{\mathrm{DR}}$ denotes $\bar{A}_{\mathrm{DR}}$ or $\bar{B}_{\mathrm{DR}}$. The control system terms are

$$\bar{\bar{P}}^c_R = \bar{P}^c_R + \bar{q}\bar{A}_{\mathrm{RD}}(K_D - \bar{q}\bar{A}_D)^{-1}\bar{P}^c_D \tag{14}$$

where $\bar{P}^c_R$ denotes $\bar{M}^c_R$, $\bar{A}^c_R$, or $\bar{B}^c_R$ and $\bar{P}^c_D$ denotes $\bar{M}^c_D$, $\bar{A}^c_D$, or $\bar{B}^c_D$.

The partitions A_R and B_R in Eq. (5) are the aerodynamic coefficients for a rigid vehicle. The partitions $\bar{A}_R$ and $\bar{B}_R$ in Eq. (7) are the mean axis DOF aerodynamic coefficients for a vehicle with the static modes residualized but not the dynamic modes. The matrices $\bar{\bar{A}}_R$ and $\bar{\bar{B}}_R$ in Eq. (12) are the mean axis DOF aerodynamic coefficients for a QSAE vehicle with no dynamic structural modes included, i.e., all modes are regarded as static. The important point to note is that $A_R \neq \bar{A}_R \neq \bar{\bar{A}}_R$ and $B_R \neq \bar{B}_R \neq \bar{\bar{B}}_R$.

The equation of motion described by Eq. (5) represents a flexible vehicle with all of its modes considered as dynamic. The equation of motion described by Eq. (7) represents a flexible vehicle with some but not all of its structural dynamic effects included. The equation of motion described by Eq. (12) represents a flexible vehicle with none of its structural dynamic effects included. This corresponds to a QSAE vehicle where all of the static flexible effects are included, but none of the dynamic flexible effects are included. This is the formulation that leads to unrestrained aeroelastic derivatives such as those obtained from FLEXSTAB[6] or MSC/NASTRAN, SOL 144 (Ref. 7). Solving for the dynamic stability (the eigenvalue problem) of each of Eqs. (5), (7), and (12) results in different mean body DOF roots, e.g., the short period root in the longitudinal case.

Let us compare Eqs. (7) and (12) and define generic increments in Eqs. (13) and (14) as

$$\bar{\bar{P}}_R = \bar{P}_R - \Delta\bar{\bar{P}}_R \tag{15}$$

where $\bar{P}_R$ denotes $\bar{A}_R$, $\bar{B}_R$, $\bar{M}^c_R$, $\bar{A}^c_R$ or $\bar{B}^c_R$ and

$$\Delta\bar{\bar{P}}_R = -\bar{q}\bar{A}_{\mathrm{RD}}(K_D - \bar{q}\bar{A}_D)^{-1}\bar{P}_{\mathrm{DR}} \tag{16}$$

where $\bar{P}_{\mathrm{DR}}$ denotes $\bar{A}_{\mathrm{DR}}$ or $\bar{B}_{\mathrm{DR}}$, or

$$\Delta\bar{\bar{P}}_R = -\bar{q}\bar{A}_{\mathrm{RD}}(K_D - \bar{q}\bar{A}_D)^{-1}\bar{P}_D \tag{17}$$

in which $\bar{P}_D = \bar{M}^c_D\, \bar{A}^c_D$, or $\bar{B}^c_D$. We may rewrite Eq. (7) using Eq. (15) to give

$$\begin{bmatrix} M_R & \vdots & 0 \\ \cdots & \vdots & \cdots \\ 0 & \vdots & M_D \end{bmatrix} \begin{Bmatrix} \ddot{q}_R \\ \cdots \\ \ddot{q}_D \end{Bmatrix} + \begin{bmatrix} 0 & \vdots & 0 \\ \cdots & \vdots & \cdots \\ 0 & \vdots & C_D \end{bmatrix} \begin{Bmatrix} \dot{q}_R \\ \cdots \\ \dot{q}_D \end{Bmatrix} + \begin{bmatrix} 0 & \vdots & 0 \\ \cdots & \vdots & \cdots \\ 0 & \vdots & K_D \end{bmatrix} \begin{Bmatrix} q_R \\ \cdots \\ q_D \end{Bmatrix}$$

$$= \bar{q} \begin{Bmatrix} Q_0 \\ \cdots \\ 0 \end{Bmatrix} + \bar{q} \begin{bmatrix} \bar{\bar{A}}_R + \Delta\bar{\bar{A}}_R & \vdots & \bar{A}_{\mathrm{RD}} \\ \cdots & \vdots & \cdots \\ \bar{A}_{\mathrm{DR}} & \vdots & \bar{A}_D \end{bmatrix} \begin{Bmatrix} q_R \\ \cdots \\ q_D \end{Bmatrix}$$

$$+ \bar{q}\left(\frac{\bar{c}}{2V}\right) \begin{bmatrix} \bar{\bar{B}}_R + \Delta\bar{\bar{B}}_R & \vdots & \bar{B}_{\mathrm{RD}} \\ \cdots & \vdots & \cdots \\ \bar{B}_{\mathrm{DR}} & \vdots & \bar{B}_D \end{bmatrix} \begin{Bmatrix} \dot{q}_R \\ \cdots \\ \dot{q}_D \end{Bmatrix} - \begin{bmatrix} \bar{\bar{M}}^c_R + \Delta\bar{\bar{M}}^c_R \\ \cdots \\ \bar{M}^c_D \end{bmatrix} \{\ddot{q}^c\}$$

$$+ \bar{q} \begin{bmatrix} \bar{\bar{A}}^c_R + \Delta\bar{\bar{A}}^c_R \\ \cdots \\ \bar{A}^c_D \end{bmatrix} \{q^c\} + \bar{q}\left(\frac{\bar{c}}{2V}\right) \begin{bmatrix} \bar{\bar{B}}^c_R + \Delta\bar{\bar{B}}^c_R \\ \cdots \\ \bar{B}^c_D \end{bmatrix} \{\dot{q}^c\} + \begin{Bmatrix} W \\ \cdots \\ 0 \end{Bmatrix} \tag{18}$$

Equation (18) is the formulation of Rodden and Love[1] if the increments $\Delta\bar{\bar{A}}_R$, $\Delta\bar{\bar{B}}_R$, $\Delta\bar{\bar{M}}^c_R$, $\Delta\bar{\bar{A}}^c_R$, and $\Delta\bar{\bar{B}}^c_R$ are set to zero. The mistake is seen in their omission. Both Eqs. (7) and (18) are correct; which is preferable depends on the analyst.

Example of a Forward-Swept Wing Airplane

A forward-swept wing airplane has been considered as an example in Refs. 1 and 7 and is reconsidered here. In Ref. 1 strip theory aerodynamics were used, and in Ref. 7 the doublet-lattice method was used. The planform with its structural, inertial, and aerodynamic idealizations is shown in Fig. 1. The structural model is shown on the right side with the grid points (GP) numbered; the doublet-lattice aerodynamic model is shown on the left side with 8 boxes on the left canard and 32 boxes on the left wing, and body interference is neglected. The airplane has a gross weight of 16,000 lb. Its wing span is 40 ft, its canard span is 10 ft, and both surfaces have chords of 10 ft. The structural damping is assumed at two percent. The canard mass and aerodynamic damping are neglected, and the intercept coefficients are assumed to be zero. The remaining characteristics are discussed in the references. This simple model has only six vibration modes for out-of-plane motion; their frequencies are 9.89, 18.40, 43.22, 56.77, 71.03, and 138.35 Hz. The example maneuver assumes a dynamic pressure of 1200 psf, which corresponds to a speed of 1005 ft/s and a Mach number of 0.90 at sea level. The airplane is in trimmed level flight for 0.10 s with an angle of attack of 0.178 deg and canard position of 1.007 deg. Then a pull-up is initiated, and the control input rotates the canard at 50 deg/s to 4.007 deg at 0.16 s. At 0.66 s a push-over is begun, and the canard position reaches -1.993 deg at 0.78 s. At 1.28 s the control is reversed and returns to the trim position at 1.34 s.

Tables 1, 2, and 3 present calculated mean axis load factor at GP 90, mean axis pitch acceleration, and first flexible modal acceleration, respectively, at selected values of time. The second column presents the accelerations of the QSAE vehicle, i.e., the solution of Eq. (12) where all six modes have been residualized. The third column shows the correct solution based on Ref. 2 with the six dynamic modes retained [equivalent to Eq. (5) with no static modes], the fourth column shows the correct solution with one dynamic mode and five residualized modes, and the fifth column shows the correct solution with one dynamic mode retained and the remaining modes truncated. The differences between the QSAE solution and the dynamic modal solutions result from the abrupt changes in the canard motion; more gradual changes would not excite the structure as much. Finally, the sixth column shows the incorrect solution of Ref. 1 with all six dynamic modes retained [equivalent to Eq. (18) with the delta increments set to zero].

The time histories of the QSAE vehicle have been plotted in Fig. 4 of Ref. 1. The various solutions in Tables 1 and 2 are slightly different, but they are not shown here. The new result for the first flexible mode, not obtained in Ref. 1 and shown in Table 3, is also plotted in Fig. 2 for the case of all six flexible modes retained in the analysis.

In this example, it is seen that only one dynamic mode is required to achieve convergence because of the wide separation between the first and second modal frequencies, and that modal residualization

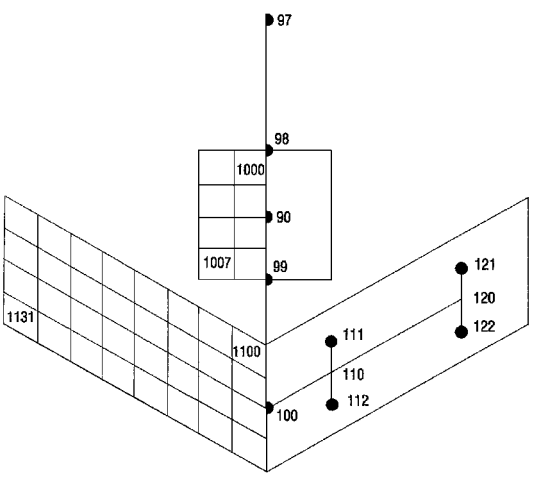

Fig. 1 Idealization of forward-swept wing airplane.

Table 1 Mean axis load factor at GP 90 (g)

t, s	QSAE	Correct solution[2] 6 modes	Correct solution Eq. (7)—1 mode 5 modes residualized	Correct solution Eq. (7)—1 mode no residual modes	Incorrect solution[1] 6 modes
0.10	1.000	1.000	1.000	1.000	1.000
0.16	2.089	1.946	1.961	1.897	2.240
0.34	4.413	4.462	4.465	4.515	4.186
0.66	3.764	3.799	3.798	3.778	3.749
0.78	0.768	0.870	0.848	1.016	0.299
0.94	−2.931	−2.952	−2.964	−3.055	−2.437
1.28	−1.836	−1.891	−1.890	−1.848	−1.773
1.34	−0.841	−0.989	−0.974	−1.067	−0.462
1.40	0.116	0.180	0.186	0.051	0.481
1.60	1.335	1.269	1.270	1.381	0.991
1.80	0.874	0.918	0.916	0.853	1.050
2.00	1.048	1.023	1.024	1.056	0.978

Table 2 Mean axis pitch acceleration (deg/s^2)

t, s	QSAE	Correct solution[2] 6 modes	Correct solution Eq. (7)—1 mode 5 modes residualized	Correct solution Eq. (7)—1 mode no residual modes	Incorrect solution[1] 6 modes
0.10	0.0	0.0	0.0	0.0	0.0
0.16	115.3	116.9	116.6	122.1	96.3
0.34	−45.5	−48.3	−48.2	−50.0	−33.5
0.66	−0.3	−3.3	−3.0	0.1	−4.2
0.78	−162.8	−159.0	−158.9	−169.9	−126.9
0.94	81.8	82.6	82.8	88.7	50.7
1.28	6.0	10.1	9.9	5.8	5.4
1.34	126.0	127.3	126.9	133.2	96.2
1.40	48.9	41.6	41.9	49.4	29.4
1.60	−18.8	−11.9	−12.4	−20.2	3.9
1.80	7.2	3.1	3.3	8.0	−4.1
2.00	−2.7	−0.7	−0.8	−3.1	1.5

Table 3 First flexible modal acceleration (g)

t, s	QSAE	Correct solution[2] 6 modes	Correct solution Eq. (7)—1 mode 5 modes residualized	Correct solution Eq. (7)—1 mode no residual modes	Incorrect solution[1] 6 modes
0.10	—	0.000	0.000	0.000	0.000
0.16	—	0.255	0.253	0.247	0.157
0.34	—	−0.301	−0.313	−0.277	−0.237
0.66	—	−0.017	−0.014	−0.003	−0.009
0.78	—	−0.218	−0.238	−0.270	−0.107
0.94	—	0.445	0.423	0.404	0.312
1.28	—	0.047	0.047	0.035	0.013
1.34	—	0.291	0.293	0.291	0.149
1.40	—	−0.044	−0.021	0.027	−0.054
1.60	—	−0.001	0.004	−0.050	0.049
1.80	—	0.001	−0.004	0.022	−0.019
2.00	—	0.002	0.003	−0.008	0.005

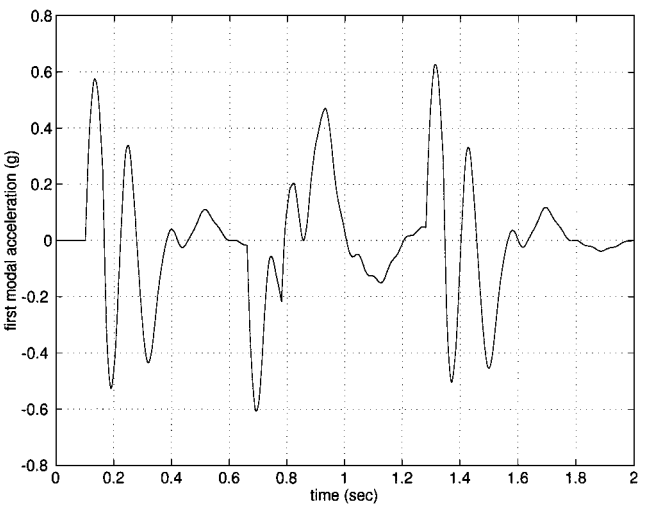

Fig. 2 First flexible modal acceleration response.

is obviously more accurate than truncation. It is also seen that the mistake in Ref. 1 is substantial.

Conclusions

The small example presented illustrates the important aspects of this Note. First, it shows the magnitude of the differences between Refs. 1 and 2, which was the primary purpose of this Note. Then, it shows the excellent accuracy of a modal solution using a limited number of modes if the higher modes are accounted for by residualization. Finally, it shows the limited accuracy of a modal solution in which the higher modes are simply truncated.

It is somewhat surprising that the formulation of Ref. 1 is incorrect (especially to its authors). It was derived using the standard approach of linear partial differential equations, which states that a general response is a superposition of a forced solution plus a homogeneous solution that damps out at large time. That approach apparently was not applied correctly as evidenced by the necessary incremental terms in Eq. (18). It has been suggested (Dusto, A. R., private communication with W. P. Rodden, Nov. 1996.) that the formulation of Ref. 1 includes the effects of flexibility twice; that

must be the case because both Eqs. (7) and (18) provide the same solution.

References

[1]Rodden, W. P., and Love, J. R., "Equations of Motion of an Elastic Flight Vehicle Utilizing Static Aeroelastic Characteristics of the Restrained Vehicle," AIAA Paper 84-0986, May 1984.

[2]Wykes, J. H., and Lawrence, R. E., "Aerothermoelasticity: Its Impact on Stability and Control of Winged Aerospace Vehicles," *Journal of Aircraft*, Vol. 2, No. 6, 1965, pp. 517–526.

[3]Sheena, Z., and Karpel, M., "Static Aeroelastic Analysis Using Aircraft Vibration Modes," *Proceedings of the 2nd International Symposium on Aeroelasticity and Structural Dynamics, 1985*, pp. 229–232; also *Israel J. Tech.*, Vol. 23, 1986, pp. 141, 142.

[4]Rodden, W. P., Giesing, J. P., and Kalman, T. P., "Refinement of the Nonplanar Aspects of the Subsonic Doublet-Lattice Lifting Surface Method," *Journal of Aircraft*, Vol. 9, No. 1, 1972, pp. 69–73.

[5]Rodden, W. P., Taylor, P. F., and McIntosh, S. C., Jr., "Further Refinement of the Nonplanar Aspects of the Subsonic Doublet-Lattice Lifting Surface Method," International Council of the Aeronautical Sciences, Paper 96-2.8.2, Sept. 1996.

[6]Dusto, A. R., et al., "A Method for Predicting the Stability Derivatives of an Elastic Airplane; Vol. I—FLEXSTAB Theoretical Description," NASA CR-114712, Oct. 1974; also Air Force Flight Dynamics Lab., TR-74-91, Vol. 1, Nov. 1974.

[7]Rodden, W. P., and Johnson, E. H., *MSC/NASTRAN Aeroelastic Analysis User's Guide*, MacNeal-Schwendler Corp., 1994.

Numerical Analysis of a Finite Wing Altered by a Leading-Edge Ice Accretion

Gregory J. Falabella* and David G. Briggs†
Rutgers University, Piscataway, New Jersey 08854-8058

Introduction

THE disastrous effects of ice accumulation on aircraft are well known. However, for preventative measures to be designed and implemented, the problem must somehow be quantified and various deicing techniques tested. Numerical simulations provide us with a relatively inexpensive way of gathering information on the performance degradation and flowfield characteristics associated with various airfoil/ice accretion shape combinations. Furthermore, they also offer the means by which the effectiveness of deicing methods can be ascertained.

Although research relating to aircraft icing dates back to the 1920s and early 1930s, most modern data have been acquired under a NASA initiative of concurrent experimental and computational research that began in 1978. Specifically, with regard to aircraft performance and flowfield evaluation, the most significant experimental work conducted under this program has been due to Bragg. Beginning his investigations in the early 1980s, Bragg has made use of two distinct shapes known as rime and glaze ice. The former develop at low temperatures and are aerodynamically shaped. Hence, the main consequence of their presence is increased drag due to surface roughness and early boundary-layer transition. On the other hand, glaze accretions, which form at temperatures at or near freezing, are highly irregular and significantly effect the aerodynamics of the flow causing premature stall and excessive drag. Bragg's work spans two decades and includes data on both iced airfoils and iced wings. (see Bragg and Coirier,[1] Bragg and Khodadoust,[2] and Khodadoust and Bragg[3]). It is highly regarded and often used to validate various flow solvers.

Numerical studies have also been performed in the hope that one day highly detailed, reliable information will be available quickly, promoting a thorough analysis of the icing problem and the subsequent development of effective deicing systems. Along this vein there have been two major players to date. The first is Cebeci who used an interactive boundary layer method to evaluate performance losses of a NACA-0012 airfoil with a simulated leading-edge ice shape.[4] Comparison of his results with experimental data indicate good agreement of global properties up to stall. Second, Potapczuk,[5] using the thin-layer Navier–Stokes solver ARC2D, predicted aerodynamic losses beyond stall for the same ice shape and obtained data suggesting that the flow is unsteady with periodic vortex shedding at angles of attack above 7 deg.

Additionally, Kwon and Sankar[6,7] have used a three-dimensional Navier–Stokes code in an effort to analyze an entire wing with leading-edge ice accretion at two different angles of attack. Although the resolution in the boundary layer was quite coarse, the predicted coefficients of lift and pressure were in good agreement with experimental data for an angle of attack of 4 deg. At 8 deg, however, results were poor and prompted further examination. It was then found that modeling of the splitter plate used in the wind tunnel improved results to the point of qualitative agreement.

The present study is a comprehensive effort involving the development and validation of a finite difference-based Navier–Stokes solver and its subsequent use to explore thoroughly the problem of performance degradation due to leading-edge ice accretion. It is a complete study[8] encompassing analysis of both two-dimensional and three-dimensional configurations with the same code. Computations are performed within a three-dimensional parametric space and account for compressibility and variations in Reynolds number. Furthermore, the solver developed is extremely robust. Results obtained from the simulations agree with all previously established experimental and numerical data. Additionally, grid convergence, grid sensitivity, and iteration convergence have been explored guaranteeing that the results obtained are valid and can be reproduced on any appropriate mesh.

In this Note, the results of a specific numerical analysis performed to ascertain the aerodynamics of a wing altered by a leading-edge glaze ice accretion are presented. The wing, made up of NACA-0012 sections, is untwisted and untapered and has an aspect ratio of five. The ice shape employed was the simulated shape used in Refs. 2 and 3, hence facilitating a one-to-one comparison with experimental data and previous computational results.

Computational Methodology

Governing Equations

The governing equations are the complete unsteady, three-dimensional Reynold's-averaged Navier–Stokes equations. To simplify application of the boundary conditions and enhance the overall accuracy of the numerical solution a body-fitted or curvilinear coordinate transformation[9] has been applied to the governing equations. The necessary metrics associated with this approach are computed from the grid using central differences for the interior nodes and second-order one-sided differences at the boundaries.

A two-layer algebraic turbulence model[10] was employed for this research with the eddy viscosity given as

$$\nu_T = l_{\text{mix}}^2 |\omega|, \qquad l_i = \kappa y[1 - \exp(-y^+/A)]$$
$$l_o = C_1 \delta, \qquad l_{\text{mix}} = \min(l_i, l_o) \tag{1}$$

The constants κ and $A+$ are the von Kármán constant and the van Driest damping coefficient and are taken as 0.41 and 26, respectively. The closure coefficient C_1 is set to 0.089, $|\omega|$ is the magnitude of the vorticity vector, and y^+ is defined as $y(|\tau_w|/\rho_w)^{1/2}/\nu_w$.

Received 11 May 1999; revision received 10 December 1999; accepted for publication 14 December 1999.

*Research Associate, Department of Mechanical and Aerospace Engineering, College of Engineering, 98 Brett Road; currently Assistant Professor, Department of Chemistry and Physics, Wagner College, 1 Campus Road, Staten Island, NY 10301. Senior Member AIAA.

†Professor Emeritus, Department of Mechanical and Aerospace Engineering, Rutgers University, College of Engineering, 98 Brett Road.